which suggests that different R proteins are activated by different mechanisms or that intermediate signaling steps are still to be identified that would lead to a similar mode of activation.

A key common point in these models is that pathogen virulence proteins are recognized as a consequence of their virulence function, rather than by direct interaction with a plant R protein. Such indirect recognition would be expected to significantly constrain the coevolution of pathogens and their plant hosts, as evasion of detection would require modification of virulence functions. Furthermore, by recognizing pathogen virulence proteins based on their enzymatic activity rather than their shape, plants could likely detect a large number of pathogen effectors with a limited number of R proteins. Although the extent of this mechanism is unknown [only three *R* genes are known to have dual specificity (*24*–*26*)], this seems an attractive strategy for the plant to maximize its surveillance capacity against the multitude of potential pathogen effectors. This may be a critical aspect of the plant immune system, as, unlike vertebrates, plants cannot generate a diversity of antibodies via somatic recombination.

AvrPphB belongs to a family of cysteine proteases found in both animal and plant pathogens (*10*), at least one of which, AvrPpiC2, is also known to induce resistance responses in specific plant genotypes (*27*). Several other bacterial Avr proteins display structural similarity to a second family of cysteine proteases (the YopJ family), and mutations in the putative catalytic residues of one of these, AvrBsT, abolish avirulence activity (*28*). Similarly, the fungal Avr protein AvrPita is homologous to known metalloproteases, and mutations in its putative catalytic residues also abolish avirulence activity (*29*). In light of our data, these observations suggest that proteolysis of host target proteins may be a common trigger for many plant *R* gene pathways.

References and Notes

1. H. H. Flor, *Phytopathology* **45**, 680 (1955).
2. J. L. Dangl, J. D. Jones, *Nature* **411**, 826 (2001).
3. Y. Jia, S. A. McAdams, G. T. Bryan, H. P. Hershey, B. Valent, *EMBO J.* **19**, 4004 (2000).
4. L. Deslandes *et al.*, *Proc. Natl. Acad. Sci. U.S.A.* **100**, 8024 (2003).
5. S. Kjemtrup, Z. Nimchuk, J. L. Dangl, *Curr. Opin. Microbiol.* **3**, 73 (2000).
6. E. A. van der Biezen, J. D. G. Jones, *Trends Biochem. Sci.* **23**, 454 (1998).
7. D. Mackey, Y. Belkhadir, J. M. Alonso, J. R. Ecker, J. L. Dangl, *Cell* **112**, 379 (2003).
8. D. Mackey, B. F. Holt, A. Wiig, J. L. Dangl, *Cell* **108**, 743 (2002).
9. M. J. Axtell, B. J. Staskawicz, *Cell* **112**, 369 (2003).
10. F. Shao, P. M. Merritt, Z. Bao, R. W. Innes, J. E. Dixon, *Cell* **109**, 575 (2002).
11. R. F. Warren, A. Henk, P. Mowery, E. Holub, R. W. Innes, *Plant Cell* **10**, 1439 (1998).
12. A. P. Tampakaki, M. Bastaki, J. W. Mansfield, N. J. Panopoulos, *Mol. Plant-Microbe Interact.* **15**, 292 (2002).
13. M. R. Swiderski, R. W. Innes, *Plant J.* **26**, 101 (2001).
14. R. F. Warren, P. M. Merritt, E. Holub, R. W. Innes, *Genetics* **152**, 401 (1999).
15. Materials and methods are available as supporting material on *Science* Online.
16. Single-letter abbreviations for the amino acid residues are as follows: A, Ala; C, Cys; D, Asp; E, Glu; F, Phe; G, Gly; H, His; I, Ile; K, Lys; L, Leu; M, Met; N, Asn; P, Pro; Q, Gln; R, Arg; S, Ser; T, Thr; V, Val; W, Trp; and Y, Tyr.
17. P. Tornero *et al.*, *Plant Cell* **14**, 1005 (2002).
18. C. Azevedo *et al.*, *Science* **295**, 2073 (2002).
19. Z. Nimchuk *et al.*, *Cell* **101**, 353 (2000).
20. N. Puri *et al.*, *Mol. Plant-Microbe Interact.* **10**, 247 (1997).
21. F. Shao, J. E. Dixon, unpublished observations.
22. J. Zhou, Y. T. Loh, R. A. Bressan, G. B. Martin, *Cell* **83**, 925 (1995).
23. J. Krüger *et al.*, *Science* **296**, 744 (2002).
24. S. R. Bisgrove, M. T. Simonich, N. M. Smith, A. Sattler, R. W. Innes, *Plant Cell* **6**, 927 (1994).
25. Y. J. Kim, N. C. Lin, G. B. Martin, *Cell* **109**, 589 (2002).
26. M. Rossi *et al.*, *Proc. Natl. Acad. Sci. U.S.A.* **95**, 9750 (1998).
27. D. L. Arnold *et al.*, *Microbiology* **147**, 1171 (2001).
28. K. Orth *et al.*, *Science* **290**, 1594 (2000).
29. M. J. Orbach, L. Farrall, J. A. Sweigard, F. G. Chumley, B. Valent, *Plant Cell* **12**, 2019 (2000).
30. *Arabidopsis* mutant alleles used in this work have been described previously (*13*, *14*, *17*). The *pbs1-1* and *rar1-20* mutations are protein null, whereas *rps5-2* and *pbs1-2* are missense mutations that display complete loss-of-function phenotypes.

31. We thank Z. Bao and R. Kruger for technical assistance; M. Swiderski for the construction of a PBS1-HA plasmid; and P. Merritt, M. Estelle, and B. Staskawicz for comments on the manuscript. F.S. was supported by the Anthony and Lillian Lu graduate student fellowship. This work was supported by National Institutes of Health grants DK18849 (J.E.D.) and GM46451 (R.W.I.), the Walther Cancer Institute (J.E.D.), and the Ellison Medical Foundation (J.E.D.).

Supporting Online Material

www.sciencemag.org/cgi/content/full/301/5637/1230/DC1

Materials and Methods
Figs. S1 to S5
References

14 April 2003; accepted 23 July 2003

Single-Molecule Measurement of Protein Folding Kinetics

Everett A. Lipman,[1]*† Benjamin Schuler,[1,2]* Olgica Bakajin,[3] William A. Eaton[1]‡

In order to investigate the behavior of single molecules under conditions far from equilibrium, we have coupled a microfabricated laminar-flow mixer to a confocal optical system. This combination enables time-resolved measurement of Förster resonance energy transfer after an abrupt change in solution conditions. Observations of a small protein show the evolution of the intramolecular distance distribution as folding progresses. This technique can expose subpopulations, such as unfolded protein under conditions favoring the native structure, that would be obscured in equilibrium experiments.

Fluorescence detection of Förster resonance energy transfer (FRET), in which the probability of excitation energy transfer between two chromophores is used to determine their separation, is a powerful tool for investigating the behavior of single biological macromolecules (*1*, *2*). Two variants of the technique are used. In the first, a dye-labeled molecule is immobilized on a surface, and its fluorescence emission is recorded continuously until one of the dyes has bleached. This allows uninterrupted observation and has been applied to both RNA and protein folding (*3*–*6*). Alternatively, fluorescence can be observed as molecules diffuse freely through the focus of a laser beam (*7*). This approach has the advantage of preventing interactions between the sample and a surface.

Free-diffusion experiments have yielded direct enumeration of thermodynamic states and information about the sizes and dynamical properties of unfolded molecules when both folded and unfolded molecules are present, information that is difficult or impossible to obtain from bulk samples (*8*–*10*). A limitation of the free-diffusion experiments performed to date is that they could only be used to examine states that are substantially populated at equilibrium. In order to study the properties of single molecules under nonequilibrium conditions, we have coupled a microfabricated laminar-flow mixer to a confocal optical system. This has allowed us to measure the FRET efficiencies of individual dye-labeled protein molecules as they flow through the illuminated volume at selected times subsequent to the triggering of folding by an abrupt change in denaturant concentration.

The microfabricated device and the sample flow in the mixing region are illustrated in Fig. 1. The mixer (*11*) is similar to that

[1]Laboratory of Chemical Physics, National Institute of Diabetes and Digestive and Kidney Diseases, Building 5, Room 104, National Institutes of Health, Bethesda, MD 20892–0520, USA. [2]Physikalische Biochemie, Universität Potsdam, 14415 Potsdam, Germany. [3]Biosecurity Nanosciences Laboratory, Chemistry and Materials Science, Lawrence Livermore National Laboratory, Livermore, CA 94550, USA.

*These authors contributed equally to this work.
†Present address: Department of Physics, University of California, Santa Barbara, CA 93106–9530, USA.
‡To whom correspondence should be addressed. E-mail: eaton@helix.nih.gov

designed by Kauffmann *et al*. (*12*) for ensemble infrared measurements. The Reynolds numbers (about 10^{-2}) in these experiments are small enough to guarantee laminar flow, and the microscopic dimensions of the mixer channels ensure that rapid mixing can occur by diffusion alone. Under these conditions, displacements due to diffusion and flow are comparable over a period of a few milliseconds, and the solutions are mixed by the time (about 50 ms) they have reached a point 50 μm beyond the center inlet.

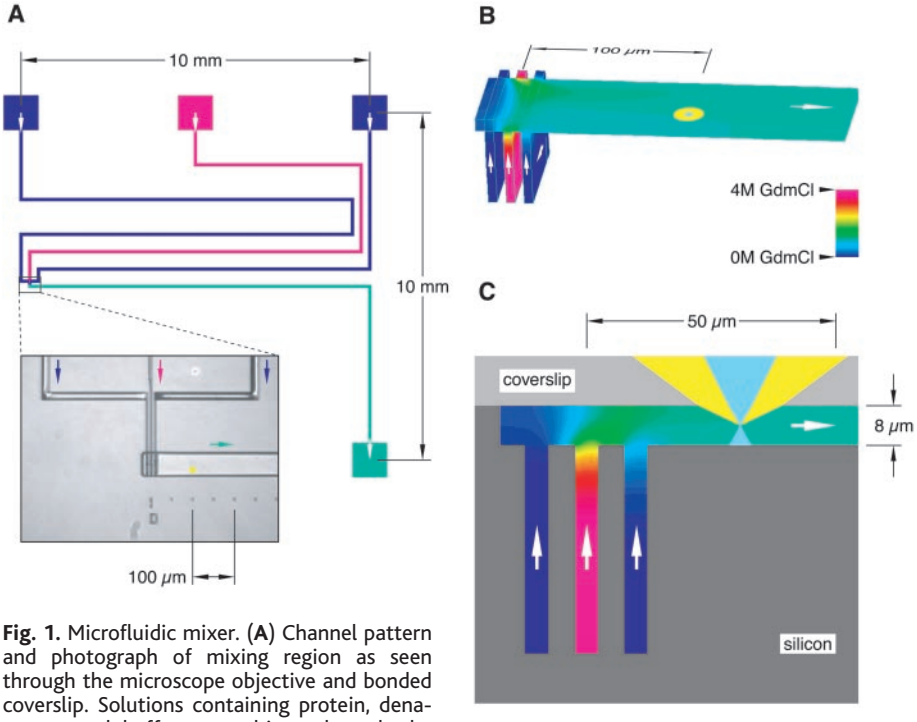

Fig. 1. Microfluidic mixer. (**A**) Channel pattern and photograph of mixing region as seen through the microscope objective and bonded coverslip. Solutions containing protein, denaturant, and buffer were driven through the channels with compressed air (*11*). Arrows indicate the direction of flow. (**B**) View of the mixing region. Computed denaturant concentration (*11*) is indicated by color. The laser beam (light blue) and collected fluorescence (yellow) are shown 100 μm from the center inlet. (**C**) Cross section of the mixing region. The $1/e^2$ intensity contour of the laser beam is illustrated along with the cone of fluorescence emission collected by the microscope objective. Actual measurements were made at distances ≥100 μm from the center inlet channel. Because the flow velocity at the vertical center of the observation channel is about 1 μm ms^{-1}, this corresponds to times ≥0.1 s.

A 488-nm laser was used to excite sample molecules in the mixer (*11*), and the resulting fluorescence was collected with an optical system identical to that used by Schuler *et al*. (*9*). The beam was positioned downstream of the mixing region at distances chosen to correspond, via the flow rate, to the desired delays. Counts from the detectors were collected in 1-ms intervals as individual molecules passed through the focal volume.

The molecule studied here is the cold shock protein (Csp) from the bacterium *Thermotoga maritima* (*11*), a small β-barrel protein that exhibits two-state thermodynamics and kinetics (*13*, *14*). Csp was labeled with a green fluorescent donor dye (Alexa Fluor 488, Molecular Probes, Eugene, Oregon) and a red fluorescent acceptor (Alexa Fluor 594) via amino- and carboxyl-terminal cysteine residues (*9*, *11*).

Representative FRET efficiency histograms measured at various times after dilution of denaturant to trigger folding are shown in Fig. 2A. The maximum at high transfer efficiency corresponds to folded molecules. For this subpopulation, excitation of the donor dye results in rapid energy transfer to the acceptor because the termini of the protein are separated by only 1 nm in the native structure (*15*). Most of the fluorescence photons are therefore emitted by the acceptor. A second maximum occurs at a transfer efficiency of about 0.5. This is produced by unfolded protein, for which the average distance between the dyes is greater. Consequently, the energy transfer rate is decreased, and the fraction of photons emitted by the acceptor is reduced.

After mixing, a redistribution of the populations is observed. As the number of un-

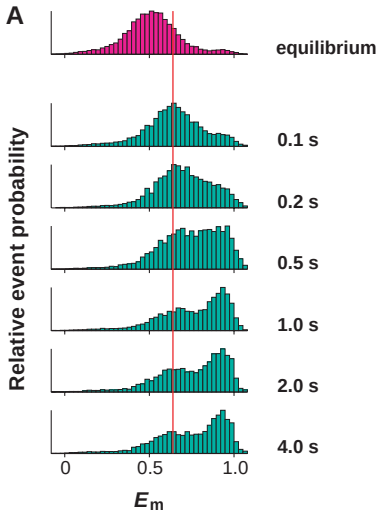

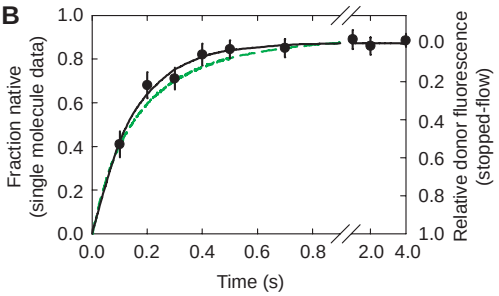

Fig. 2. (**A**) Histograms of measured FRET efficiency, E_m, during folding. (Top) The E_m distribution at equilibrium before mixing. The vertical red line indicates the mean value for E_m in the unfolded state after mixing. Measurements of E_m were taken (typically for 30 minutes) at various distances from the mixing region and thus at various times after the change in GdmCl concentration. Data collection and analysis were carried out as previously described (*9*, *11*). (**B**) Comparison of single-molecule and ensemble folding kinetics (*11*). The decrease in donor fluorescence from stopped-flow experiments is shown in green. Single-molecule data are represented by filled circles, with a corresponding single exponential fit (black). The fit to the single-molecule data has a rate constant of 6.6 ± 0.8 s^{-1}, in agreement with the result from ensemble measurements (5.7 ± 0.4 s^{-1}). Measurements of Csp unfolding are shown in fig. S2.

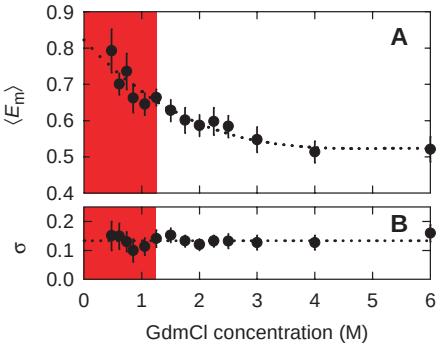

Fig. 3. Dependence of (**A**) the mean values $\langle E_m \rangle$ and (**B**) peak widths (σ) of E_m histograms for unfolded Csp as a function of GdmCl concentration. Peak widths are standard deviations of Gaussian fits. Data were obtained from single-molecule measurements in the microfluidic mixer. The dotted lines show a third-degree polynomial fit to the data (A) or indicate their mean value (B). The colored region indicates the range of denaturant concentrations where reliable data cannot be obtained from corresponding equilibrium experiments.

folded molecules decreases, there is a corresponding increase in the number of folded molecules (Fig. 2A), and eventually the distribution converges to its equilibrium form at the final concentration of denaturant. The positions of the peaks, however, remain constant, indicating that the average end-to-end distances of the molecules in the subpopulations do not change significantly during the course of the reaction. This is the behavior expected for a two-state system, as inferred for this protein from ensemble methods (*13*, *14*). The fidelity of the technique for measuring accurate kinetics is demonstrated in Fig. 2B, which shows that nearly identical folding rates are obtained from single-molecule data and ensemble stopped-flow measurements.

Whereas the peak positions are constant during the folding reaction, the mean FRET efficiency of unfolded molecules is shifted from 0.51 in the presence of 4 M guanidinium chloride (GdmCl) to 0.64 after mixing is complete and solution conditions are conducive to folding (Fig. 2A). The lower denaturant concentration after dilution results in more compact unfolded molecules, which exhibit higher FRET efficiency. For a Gaussian chain (*16*), this shift would correspond to a decrease in the radius of gyration of about 20% (*9*), which implies a halving of occupied volume. This reconfiguration is obviously complete by the time of the first observation at about 100 ms, consistent with ensemble measurements on other proteins that show collapse of unfolded molecules to be a submillisecond process (*17*–*21*). It is noteworthy that qualitatively different signal changes result from collapse and folding. Collapse of the unfolded state causes a shift of the corresponding peak to higher efficiency, whereas folding increases the folded state population (represented by peak height) and depopulates the unfolded state. This permits separate observations of the two processes. In an ensemble FRET experiment, both collapse and folding would result in an overall increase of the transfer efficiency, and the respective contributions could be identified only indirectly by kinetic modeling.

The power of single-molecule measurements is in the ability to resolve and analyze the properties of subpopulations. The kinetic experiment presented here extends the scope of the technique so that such subpopulations can be studied under conditions far from equilibrium, where they exist only briefly. Experiments in the absence of flow have shown that unfolded Csp must reconfigure quickly relative to the observation time of about 1 ms (*9*), in that no broadening of the measured energy transfer distributions was observed beyond that seen for rigid polyproline peptides. These equilibrium measurements were limited to solution conditions that resulted in sufficiently high concentrations of unfolded molecules. By transiently populating the denatured state with the microfluidic mixer, we can now extend the observations to denaturant concentrations that strongly favor the native structure and are therefore closer to physiologically relevant conditions. The present results (Fig. 3) show that the unfolded peak width is constant to GdmCl concentrations as low as 0.5 M, indicating that, even though there is significant compaction of the unfolded state between 6.0 M and 0.5 M GdmCl, there is no increase in the reconfiguration time beyond the previously calculated limit of 0.2 ms (*22*).

References and Notes

1. T. Ha *et al*., *Proc. Natl. Acad. Sci. U.S.A.* **93**, 6264 (1996).
2. S. Weiss, *Science* **283**, 1676 (1999).
3. X. Zhuang *et al*., *Science* **288**, 2048 (2000).
4. X. Zhuang *et al*., *Science* **296**, 1473 (2002).
5. Y. W. Jia *et al*., *Chem. Phys.* **247**, 69 (1999).
6. E. Rhoades, E. Gussakovsky, G. Haran, *Proc. Natl. Acad. Sci. U.S.A.* **100**, 3197 (2003).
7. A. A. Deniz *et al*., *Proc. Natl. Acad. Sci. U.S.A.* **96**, 3670 (1999).
8. A. A. Deniz *et al*., *Proc. Natl. Acad. Sci. U.S.A.* **97**, 5179 (2000).
9. B. Schuler, E. A. Lipman, W. A. Eaton, *Nature* **419**, 743 (2002).
10. D. S. Talaga *et al*., *Proc. Natl. Acad. Sci. U.S.A.* **97**, 13021 (2000).
11. Materials and methods are available as supporting material on *Science* Online.
12. E. Kauffmann, N. C. Darnton, R. H. Austin, C. Batt, K. Gerwert, *Proc. Natl. Acad. Sci. U.S.A.* **98**, 6646 (2001).
13. D. Perl *et al*., *Nature Struct. Biol.* **5**, 229 (1998).
14. D. Wassenberg, C. Welker, R. Jaenicke, *J. Mol. Biol.* **289**, 187 (1999).
15. The Förster radius R_0 (*11*, *23*) for the dye pair used here is ≈5.4 nm.
16. M. Doi, *Introduction to Polymer Physics* (Oxford, New York, 1996).
17. C. K. Chan *et al*., *Proc. Natl. Acad. Sci. U.S.A.* **94**, 1779 (1997).
18. M. C. R. Shastry, H. Roder, *Nature Struct. Biol.* **5**, 385 (1998).
19. L. Pollack *et al*., *Proc. Natl. Acad. Sci. U.S.A.* **96**, 10115 (1999).
20. S. J. Hagen, W. A. Eaton, *J. Mol. Biol.* **301**, 1019 (2000).
21. S. J. Hagen, C. W. Carswell, E. M. Sjolander, *J. Mol. Biol.* **305**, 1161 (2001).
22. B. Schuler, E. A. Lipman, W. A. Eaton, *Nature* **421**, 94 (2003).
23. B. W. VanDerMeer, G. Coker, S. Y. S. Chen, *Resonance Energy Transfer: Theory and Data* (Wiley, New York, 1994).

24. We thank R. Austin for essential advice and encouragement, K. Schwab for help with microfabrication, and S. Hagen for suggestions regarding the flow system. B.S. was supported by an Emmy Noether fellowship from the Deutsche Forschungsgemeinschaft. O.B.'s work was performed under the auspices of the U.S. Department of Energy under contract no. W-7405-Eng-48 with funding from the Laboratory Directed Research and Development program.

Supporting Online Material

www.sciencemag.org/cgi/content/full/301/5637/1233/DC1
Materials and Methods
Figs. S1 and S2

7 April 2003; accepted 18 July 2003

Single-Molecule Kinetics of λ Exonuclease Reveal Base Dependence and Dynamic Disorder

Antoine M. van Oijen,[1] Paul C. Blainey,[1] Donald J. Crampton,[2] Charles C. Richardson,[2] Tom Ellenberger,[2] X. Sunney Xie[1]*

We used a multiplexed approach based on flow-stretched DNA to monitor the enzymatic digestion of λ-phage DNA by individual bacteriophage λ exonuclease molecules. Statistical analyses of multiple single-molecule trajectories observed simultaneously reveal that the catalytic rate is dependent on the local base content of the substrate DNA. By relating single-molecule kinetics to the free energies of hydrogen bonding and base stacking, we establish that the melting of a base from the DNA is the rate-limiting step in the catalytic cycle. The catalytic rate also exhibits large fluctuations independent of the sequence, which we attribute to conformational changes of the enzyme-DNA complex.

Recent advances in single-molecule enzymatic assays have profoundly changed how biochemical reactions are studied (*1*–*7*). With the removal of ensemble averaging, distributions and fluctuations of molecular properties can be characterized, transient intermediates identified, and catalytic mechanisms elucidated. Here, we report a simple and multiplexed single-molecule assay for studying the mechanisms and dynamics of nucleic acid enzymes.

Individual DNA molecules are attached at one end to a glass surface by a biotin-streptavidin linkage and at the opposite end to polystyrene beads by a digoxigenin-antidigoxigenin linkage (*8*). When a laminar

[1]Department of Chemistry and Chemical Biology, Harvard University, 12 Oxford Street, Cambridge, MA 02138, USA. [2]Department of Biological Chemistry and Pharmacology, Harvard Medical School, 240 Longwood Avenue, Boston, MA 02115, USA.

*To whom correspondence should be addressed. E-mail: xie@chemistry.harvard.edu

Supporting Online Material for Single Molecule Measurement of Protein Folding Kinetics

Everett A. Lipman,[1,2*] Benjamin Schuler,[1,3*] Olgica Bakajin[4], William A. Eaton[1†]

[1]NIDDK Laboratory of Chemical Physics, NIH
Building 5 Room 116, Bethesda, MD 20892-0520, USA
[2]Present address: Department of Physics, University of California, Santa Barbara, CA 93106-9530.
[3]Physikalische Biochemie, Universität Potsdam, Germany
[4]Biosecurity Nanosciences Laboratory, CMS, Lawrence Livermore National Laboratory

[*]These authors contributed equally to this work.
[†]To whom correspondence should be addressed; E-mail: eaton@helix.nih.gov.

Materials and Methods

Protein

Figure S1 illustrates the dye-labeled cold shock protein (Csp) from *Thermotoga maritima*.

Microfluidic Mixer

A pattern of channels (Fig. 1) was cut into the surface of a silicon wafer using reactive ion etching. The channel depths varied from 8 μm to 50 μm, and the widths were between 5 μm and 50 μm. The observation channel, at one end of which the solutions were mixed, was

8 μm deep, 50 μm wide, and 10 mm long. Hash marks were etched adjacent to the observation channel at 50 μm intervals so that the distance from the mixing region could be accurately determined.

The concentration profiles shown in Figure 1 were modeled using pressure-determined steady-state laminar flow and sample and denaturant diffusion constants of 10^{-6} cm^2/s (= 0.1 μm^2/ms) and 10^{-5} cm^2/s (= 1 μm^2/ms), respectively. Computations were done using CFD-ACE+ software (CFDRC, Huntsville, AL).

Fluid entry to and exit from the mixer took place through four pyramidal holes, etched (using KOH) through the silicon wafer at the ends of the three inlet channels and the outlet channel. The mixer chip was clamped by its edges to a fixture that provided face-type static O-ring seals to the holes via the bottom side of the chip. For folding, a 50 mM pH 7 phosphate buffer solution was introduced in the two outer inlet channels, and a solution containing 75 pM labeled Csp, 4 M guanidinium chloride (GdmCl, Pierce Sequanal Grade), 0.01% polyoxyethylene sorbitan monolaurate (Pierce Surfact-Amps 20, "Tween 20") by volume (to prevent protein adhesion to the mixer walls), and 50 mM pH 7 phosphate buffer was placed in the center inlet channel. The pressure of the three inlets was held at 6.9 kPa above that of the outlet using a precision mechanical regulator. This resulted in a flow rate at the center of the observation channel of approximately 1 mm/s. The three inlet channels terminate at the upstream end of the observation channel (Fig. 1), where the solutions are mixed.

A 170 μm-thick 7740 Pyrex coverslip was anodically bonded to the top of the silicon device in order to seal the channels and provide a transparent window for laser excitation and fluorescence collection. Although Pyrex is well-suited for bonding directly to silicon, it produces roughly an order of magnitude more fluorescence background than an equal thickness of fused silica. This introduces additional uncertainty in the absolute determination of transfer efficiencies. A mixer fabricated from fused silica would therefore be very desirable for future

work of this type.

Mixer function was confirmed by tests that measured unfolding of labeled Csp (Fig. S2).

Data Analysis

Comparisons of the low-count tails of many raw signal histograms with Poisson distributions were used to determine the ratio of the background level to the average signal level. This number (≈ 0.75 in the present experiments) was found not to vary substantially from measurement to measurement or between the two channels. The ratio was then used to estimate the background level in each channel for a given data set. Background levels obtained in this manner were consistent with those found during manually identified intervals when no molecule was present in the focal region. Although this method is only a first-order approximation, it gives more accurate results than would a measurement of blank control solution since much of the background is caused by out-of-focus sample molecules.

After background subtraction, the sums of donor counts (n_{d}) and acceptor counts (n_{a}) for each single molecule event were used to compute measured values of the energy transfer efficiency $E_{\mathrm{m}} = \frac{n_{\mathrm{a}}}{n_{\mathrm{a}}+\gamma n_{\mathrm{d}}}$, where γ is a factor that accounts for differences in the fluorophore quantum yields and the detection efficiencies of the two channels. Based on calibration measurements (*1*), we set $\gamma = 1$. The actual transfer efficiency E (as opposed to the measured value E_{m}, which is broadened by many sources of uncertainty), can be related to the distance r between the fluorophores using Förster's theory (*2*): $E = \frac{1}{1+(r/R_0)^6}$

Ensemble Measurements

Ensemble folding kinetics were measured in a DX.18MV sequential mixing stopped-flow spectrometer (Applied Photophysics, Leatherhead, UK) with an R6094 photomultiplier tube (Hamamatsu, Bridgewater, NJ) by following the change in donor fluorescence beyond 495 nm upon

excitation at 450 nm. To initiate refolding, a 1 μM solution of labeled protein unfolded in 4 M GdmCl was diluted 11-fold with aqueous buffer or GdmCl solutions of varying concentrations to give the desired final GdmCl concentrations. Five to fifteen kinetic traces were averaged and fit to single exponentials.

Relative populations measured in the single molecule experiments can be distorted, for example by the smaller diffusion constant of protein in the unfolded state, which leads to a disproportionately large number of events in the unfolded data peak. A comparison of the ensemble equilibrium unfolding transition with single molecule equilibrium FRET efficiency histograms was used to obtain the actual fraction of native protein at each time during the folding experiment. Ensemble donor and acceptor fluorescence were measured as functions of equilibrium denaturant concentrations. As denaturant concentration increases, donor fluorescence increases and acceptor fluorescence decreases. The midpoints of the donor and acceptor transitions coincide, and measured intensities were fit with a two state model (*1*) in order to find the folded and unfolded populations at given denaturant concentrations. Equilibrium single-molecule transfer efficiency distributions were then examined to see what peak height ratio corresponded to the given population ratio from the fit.

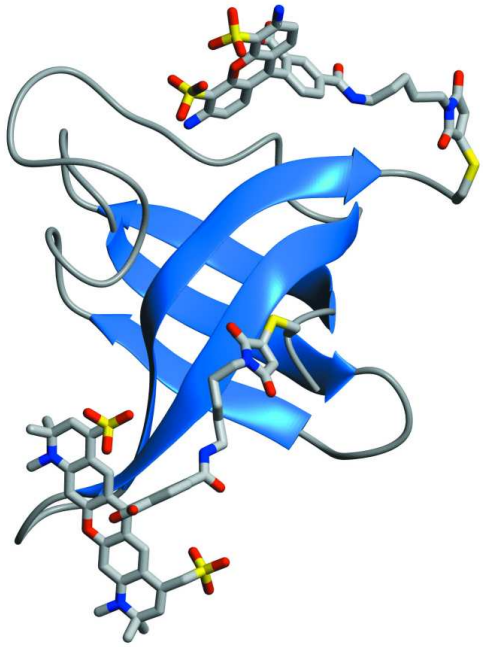

Figure S1: Representation of Csp based on the solution NMR structure (*3*, *4*). The protein is labeled with fluorescent donor and acceptor dyes at the sulfhydryl groups of the terminal Cys residues. Alexa Fluor 488 (donor, top) and Alexa Fluor 594 (acceptor, bottom) are shown here in arbitrary orientations. In the native state, the termini of the protein are separated by 1 nm.

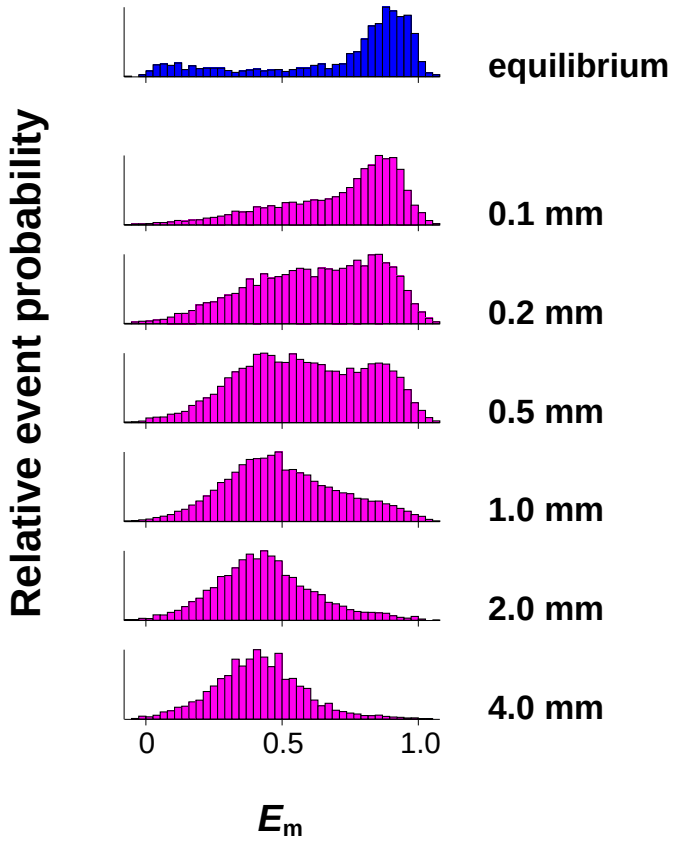

Figure S2: Histograms of measured FRET efficiency E_{m} during unfolding. A solution of labeled Csp in phosphate buffer (center inlet channel) was mixed with 8 M GdmCl (two outer inlet channels), and observations were made at the indicated distances from the mixing region. Unfolding is clearly evinced by the increase in event probability at lower transfer efficiency (greater dye-dye separation) as the reaction progresses.

References and Notes

1. B. Schuler, E. A. Lipman, W. A. Eaton, *Nature* **419**, 743 (2002).

2. B. W. VanDerMeer, G. Coker, S. Y. S. Chen, *Resonance Energy Transfer: Theory and Data* (Wiley, 1994).

3. W. Kremer, *et al.*, *Europ. J. Biochem.* **268**, 2527 (2001).

4. R. Koradi, M. Billeter, K. Wüthrich, *J. Mol. Graphics* **14**, 51 (1996).